Proceedings, 6th African Rift Geothermal Conference
Addis Ababa, Ethiopia, 2nd – 4th November 2016

# DRONES IN GEOTHERMAL EXPLORATION: THERMAL INFRARED IMAGERY, AERIAL PHOTOS AND DIGITAL ELEVATION MODELS

**Mark Harvey[1], Colin Harvey[1], Julie Rowland[2] and Katherine Luketina[3]**
[1]Harvey Consultants Limited
[2]School of Environment, University of Auckland, Auckland, New Zealand,
[3]Waikato Regional Council, Private Bag 3038, Waikato Mail Centre, Hamilton 3240,

mark@harveygeoscience.co.nz

## ABSTRACT

Drones are now routinely used for collecting aerial imagery and creating digital elevation models (DEM). Lightweight thermal sensors provide another payload option for generation of very high resolution aerial thermal orthophotos. This technology allows for the rapid, safe and cost-effective survey of thermal areas, often present in inaccessible or dangerous terrain. Here we present georeferenced, temperature-calibrated thermal orthophotos of geothermal areas in the Taupo Volcanic Zone, New Zealand. Temperature calibration of the imagery allowed estimation of heat loss from thermal areas. Aerial photos and digital elevation models were also produced for these areas, with ground resolution and horizontal position error comparable to commercially produced LiDAR and aerial imagery obtained from manned aircraft. Our results show that thermal imagery collected by drones has the potential to become a key tool in geothermal science, including geological, geochemical and geophysical surveys, environmental baseline and monitoring studies, geotechnical studies and civil works.

## 1. INTRODUCTION

Photogrammetry is a technology that allows the reconstruction of three dimensional information (i.e. Digital Elevation Models) from a mosaic of overlapping, two dimensional photographs (Westoby et al., 2012). Although photogrammetry is not a new technology, recent advances in Unmanned Aerial Vehicle (UAV or drones) equipped with global positioning systems (GPS) and digital cameras have reduced the cost of collecting imagery. Modern desktop and cloud computing power allows for routine post processing of large numbers of individual image photos. The individual photos are combined into aerial orthophotos and Digital Elevation Models (DEM) of comparable quality (<0.1m) to airborne LiDAR (Harwin & Lucieer, 2012; Fonstad et al., 2013).

In volcanology, UAV have been used previously as a sensor platform for data collection in volcanic plumes (McGonigle et al., 2008). Lightweight thermal sensors provide another payload option for generation of very high resolution aerial thermal orthophotos. This technology promises to allow the rapid and safe survey of thermal areas, often present in inaccessible or dangerous terrain.

In this study we provide results from a thermal infrared and Red Green Blue (RGB) survey of the Waikite Valley thermal area, New Zealand. The survey was undertaken using a UAV equipped with a point and shoot digital camera for standard visible images (RGB), and a thermal infrared camera. The Waikite survey area is administered by the New Zealand Department of Conservation (DOC) and comprises a topographically steep and partly inaccessible valley of regenerating native wetland vegetation within the Waikite geothermal area. Thermal features are associated with the active Paeroa Fault (Berryman et al., 2008) and include high flow-rate boiling springs in the south, warm lakes in the north, hot seeps and steaming ground (Glover et al., 1992). Advective heat loss from the Waikite

Valley was previously estimated (43 MW, Glover et al., 1992)(46MW; Healy, 1952) based on flow from the Otamakokore thermal stream flow, which comprises nearly all surface out-flow from the survey area.

The purpose of this study was to assess the usefulness of drone technology for finding warm springs or other thermal features in difficult terrain such as wetlands and dense scrub, and to provide an estimate of surface heat loss from thermal water in the survey area.

# 1 METHODS

## 1.1 Field Methods

Imagery was collected using a modified DJI Phantom 2 Vision+ quadcopter (Figure 1). The quadcopter was modified by the replacement of the stock camera with an ICI 640x480 uncooled thermal sensor (spectral response 7-14µm) with automated image capture (ICI UAV module®). A Canon S100 point and shoot camera was fitted for normal visible (RGB) and DEM outputs (Harvey et al., 2014).

Figure 1: DJI Phantom 2 Vision Plus quadcopter modified with ICI thermal camera and UAV module

See Harvey et al. (2016) for a full description of the methodology used for flight planning, thermal image calibration and positional ground control.

## 1.2 Image Processing and Analysis

Two-dimensional Thermal and RGB images were converted to 3-dimensional point clouds using Agisoft Photoscan® commercial photogrammetry software, running on a Hewlett Packard laptop computer equipped with an i7 processor and 32GB RAM. Processing provided georeferenced, thermal and RGB raster orthophotos, and a DEM (Table 1).

Raster imagery was analysed and post-processed using QGIS open-source desktop geographic information system (GIS). Post processing steps included conversion of the raw pixel values to calibrated temperature values (°C), and then to heat flux values (W $m^{-2}$), as described below.

## 1.3 Estimation of Heat Loss

Areas of surface thermal water (lakes, streams) were selected from temperature calibrated raster images. For this purpose, the QGIS Raster Calculator tool was used to select pixels above the ambient temperature (8-16°C). Mean heat loss (W $m^{-2}$) from these areas was estimated using deterministic heat flow equations (Dawson, 1964; Dawson and Dickinson, 1970; Sorey and Colvard,

1994; Fridriksson et al., 2006) within a stochastic Monte Carlo simulation (Robert and Casella, 2013) developed in Microsoft Excel; randomly generated climatic data provided ambient conditions required by the equations (ambient air temperature, wind speed, humidity, air pressure)[see Harvey et al.(2016) for a full description of the methodology used to estimate heat flow].

## 2 RESULTS

For thermal imagery, 17 flights were made between 14th October and 2nd November 2015. Flight conditions were clear and cool (8-16°C) in the early morning (between 6 and 10am), with a maximum wind speed of ~6 m/s. The total flight time was about 200 min, providing 5882 thermal images. Computer post-processing of imagery took about 48 hours, providing a thermal orthophoto with a total coverage of ~2.2 $km^2$ and ground resolution of 19 cm (Figure 2)(Table 1). Manual cross checking alignment of the thermal orthophoto with the visible orthophoto indicates positional root mean squared error (RMSE) of 1.0 m for the thermal image (average offset from the visible orthophoto based on 25 evenly distributed check points). Thermal features are clearly identifiable in the thermal orthophoto.

Thermal imagery was calibrated by ground truthing; hot and cold pools of water were measured with a temperature probe just after flying. This has allowed the generation of calibrated and georeferenced thermal imagery that can be investigated in detail and analysed with standard GIS software (ArcGIS, QGIS, etc.). Calibration showed a linear relationship between pixel value and measured temperatures (Figure 7). Increased scatter was observed at higher temperatures (>80°C) that may be due to screening by steam. However, the correlation in the cross plot is good ($r^2$ = 0.98), with a standard error of the regression of ± 2.3°C under 80°C (>99.9% of thermal water surface area in the survey area is <80°C). The regression equation allowed temperature to be estimated for each pixel (Figure 2).

Lake Puakohurea is expanded in Figure 5 - Figure 6 to illustrate the quality of the thermal imagery, and thermal calibration of pixels (see Figure 7). Figure 5 indicates Lake Puakohurea is warmest (43ºC) where hot springs enter the eastern side, then cools towards the western outflow. Springs at the eastern side were measured previously (47.5 ºC; Glover et al., 1992). Figure 5(a) illustrates the selection of pixels above ambient temperature using the QGIS Raster Calculator tool (1.3), and application of heat flow equations (Figure 5b) to these pixels. Calibrated thermal imagery and Monte Carlo analysis provided heat loss (39.3 ± 10.5 MW) for thermal lakes and streams in the southern half of the survey area (including and south of Lake Puakohurea). Lakes and streams in the northern half of the survey area provided a minor component (3.7 ± 1.4 MW) of the total heat loss (43.0 ± 11.9 MW)[see Harvey et al.(2016) for detailed heat flow results].

Table 1: Image processing output

| Description | Ground Resolution (m) | RMS Error (m) | Area ($km^2$) | Computer Processing Time (hours) |
|---|---|---|---|---|
| Temperature calibrated thermal | 0.19 | ~1 (x), ~1 (y) | 2.2 | 48 |
| Georeferenced RGB orthophoto | 0.04 | 0.11 (x), 0.07(y) | 3.0 | 70 |
| Georeferenced DEM | 0.17 | 0.11 (x), 0.07(y), 0.24 (z) | 3.0 | - |

For the visible imagery and the DEM, 8 flights were made between the 7th and 10th October 2015. Flight conditions were clear and sunny, with maximum wind speed of ~8 m/s. The total flight time was about 120 minutes, providing 2035 images. Computer post-processing of imagery took about 72 hours, providing 33 orthophoto tiles and DEM with a total coverage of ~3 $km^2$, and orthophoto ground resolution of 4 cm (Figure 3 - Figure 4, Figure 6) (Table 1). Close inspection of the orthophoto allows different types of vegetation to be identified (e.g. fern, grass, blackberry, flax). Ground control check points provided Root Mean Squared (RMS) (x axis:11 cm, y axis: 7cm and z axis: 24cm).

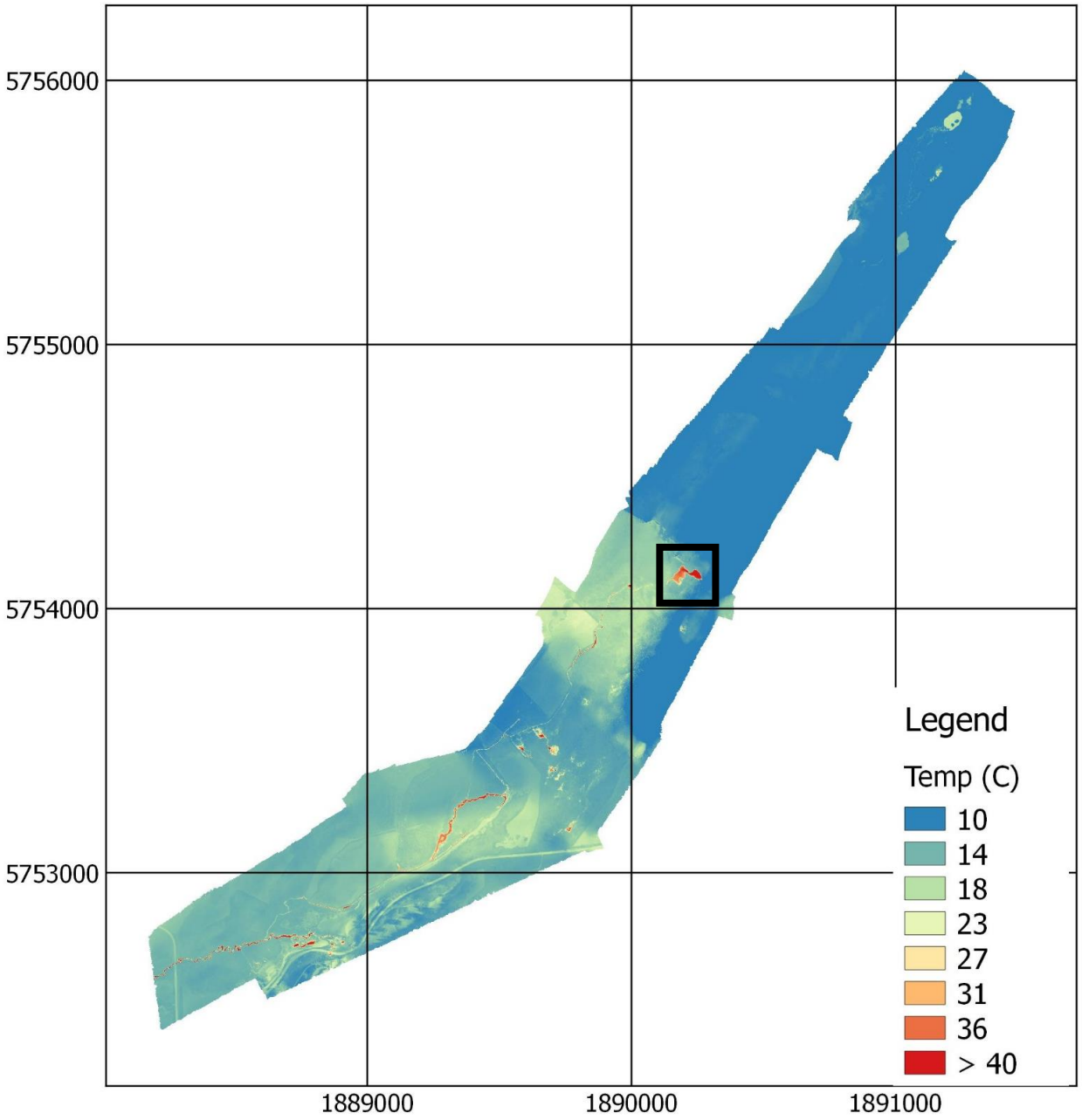


Figure 2: Waikite calibrated thermal infrared orthophoto. Black box is expanded in Figure 5(a) and (b). Map Datum NZGD2000.

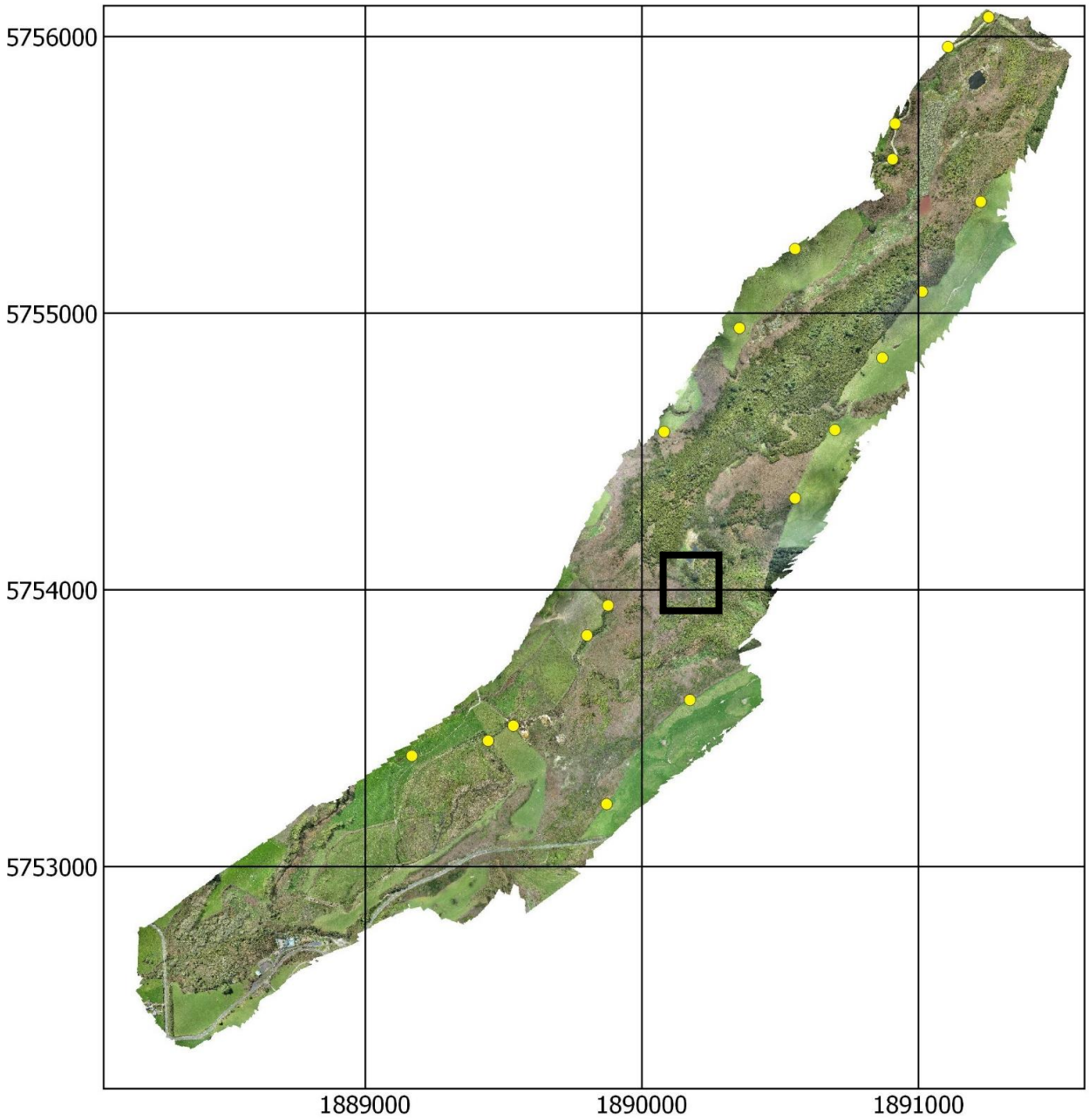


Figure 3: Waikite RGB orthophoto. Yellow dots show location of ground control points. Area within black box is expanded in Figure 5(a) and (b). Map Datum NZGD2000.

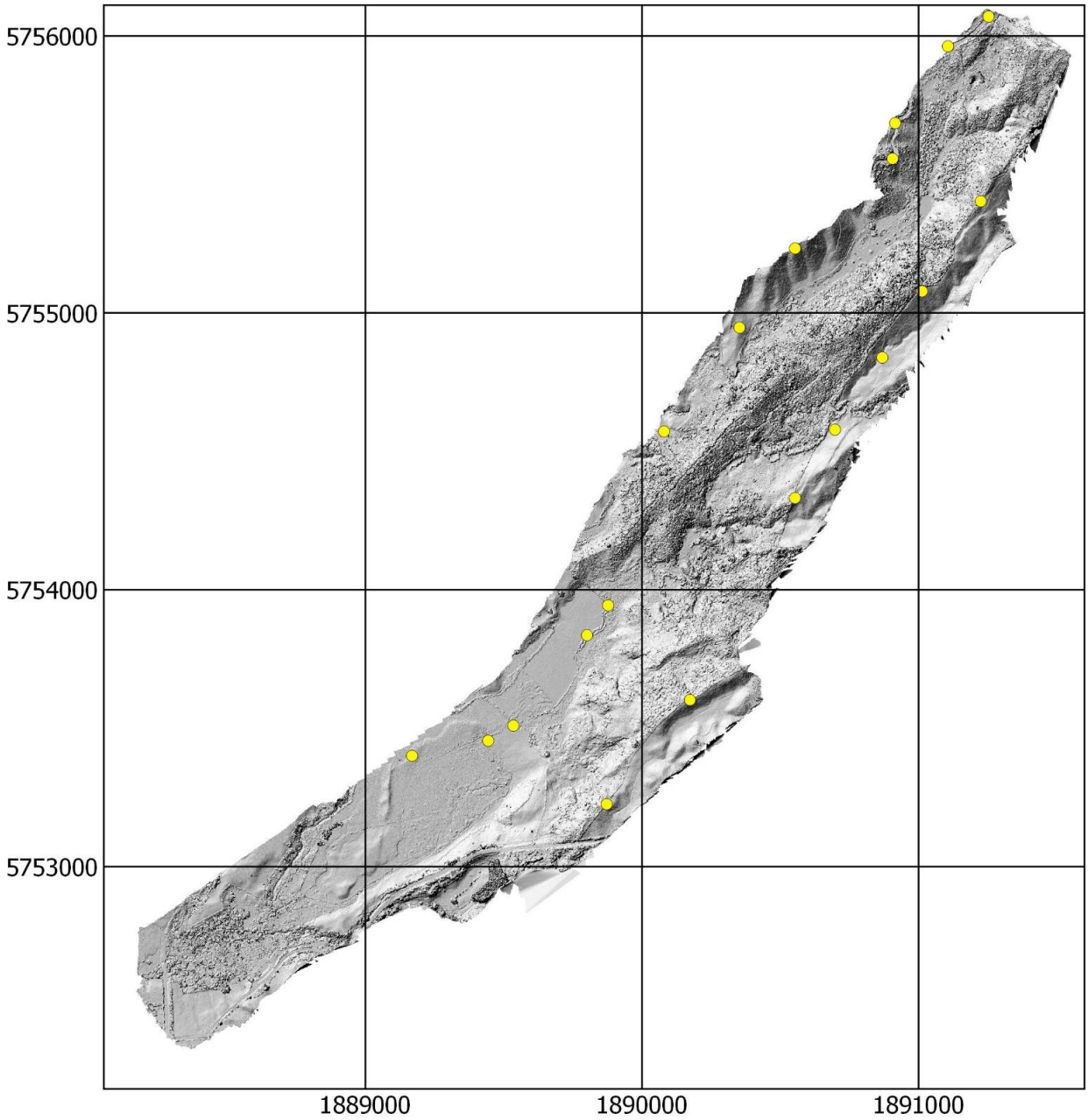


Figure 4: Waikite digital elevation model (DEM). Yellow dots show location of ground control points. Map Datum NZGD2000.

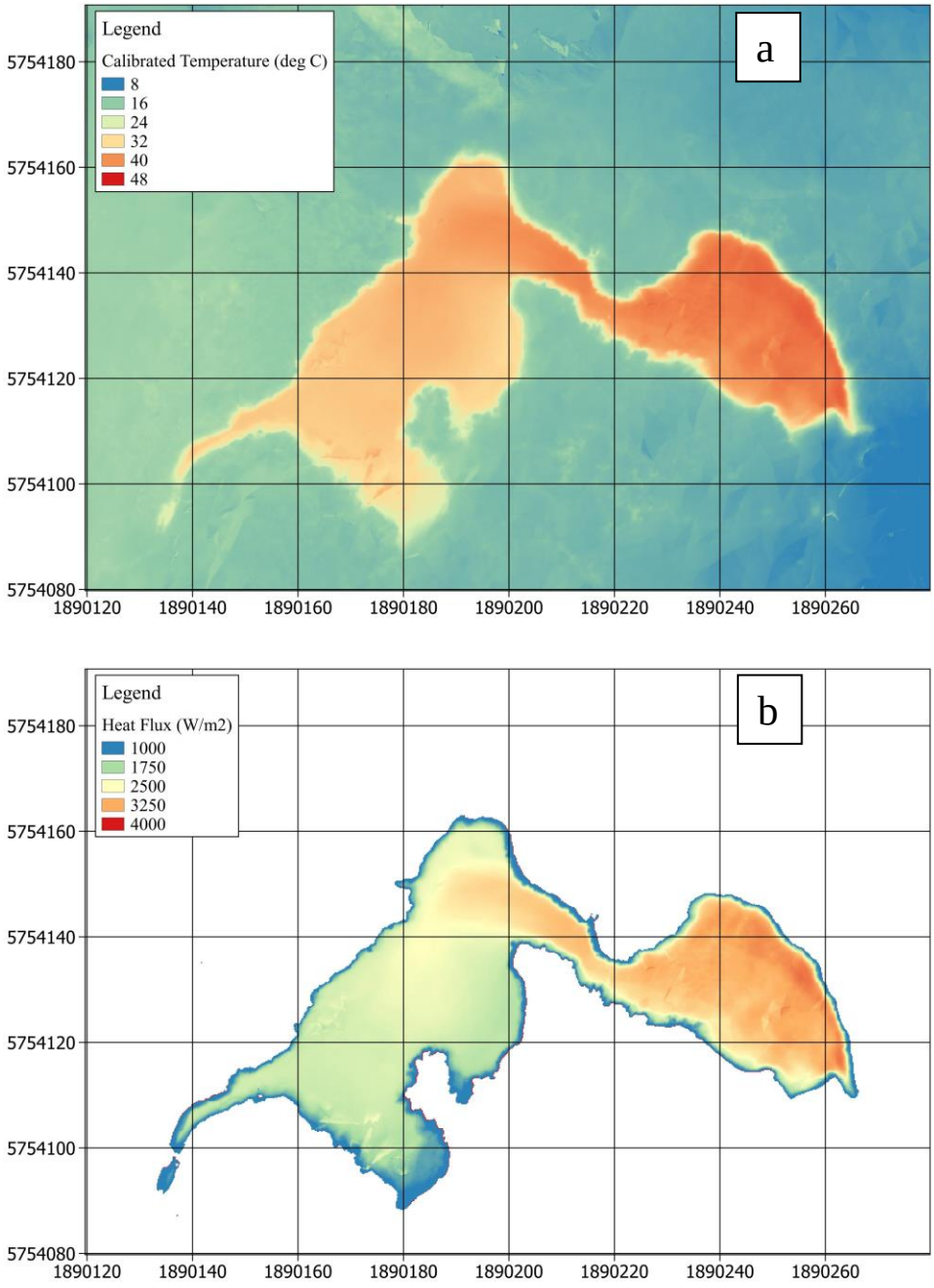


Figure 5: Expanded area showing (a) temperature calibrated, and (b) heat flux imagery of Lake Puakohurea in inaccessible terrain (19cm pixel size)(see black box Figure 2). Map Datum NZGD2000. Note: Lake is 43ºC where springs inflow (eastern side of the lake), then cools as it flows to the western outflow.

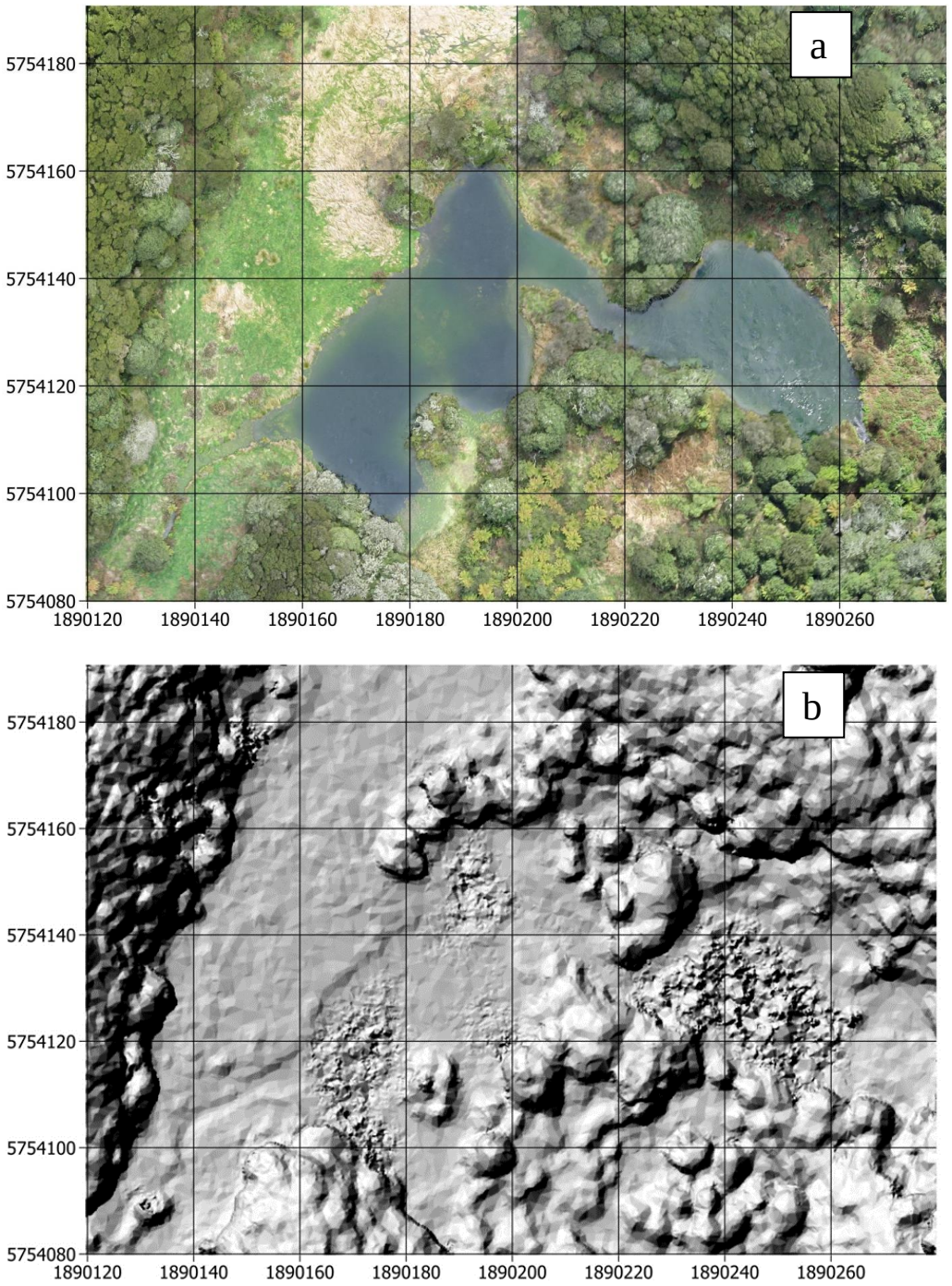


Figure 6: Expanded area showing high resolution (a) visible imagery, and (b) DEM of Lake Puakohurea in inaccessible terrain (4cm pixel size) (see black box in Figure 3). Map Datum NZGD2000. Note: irregular texture of DEM on lake surface is an artifact of the photogrammetry method; water does not provide a stationary surface.

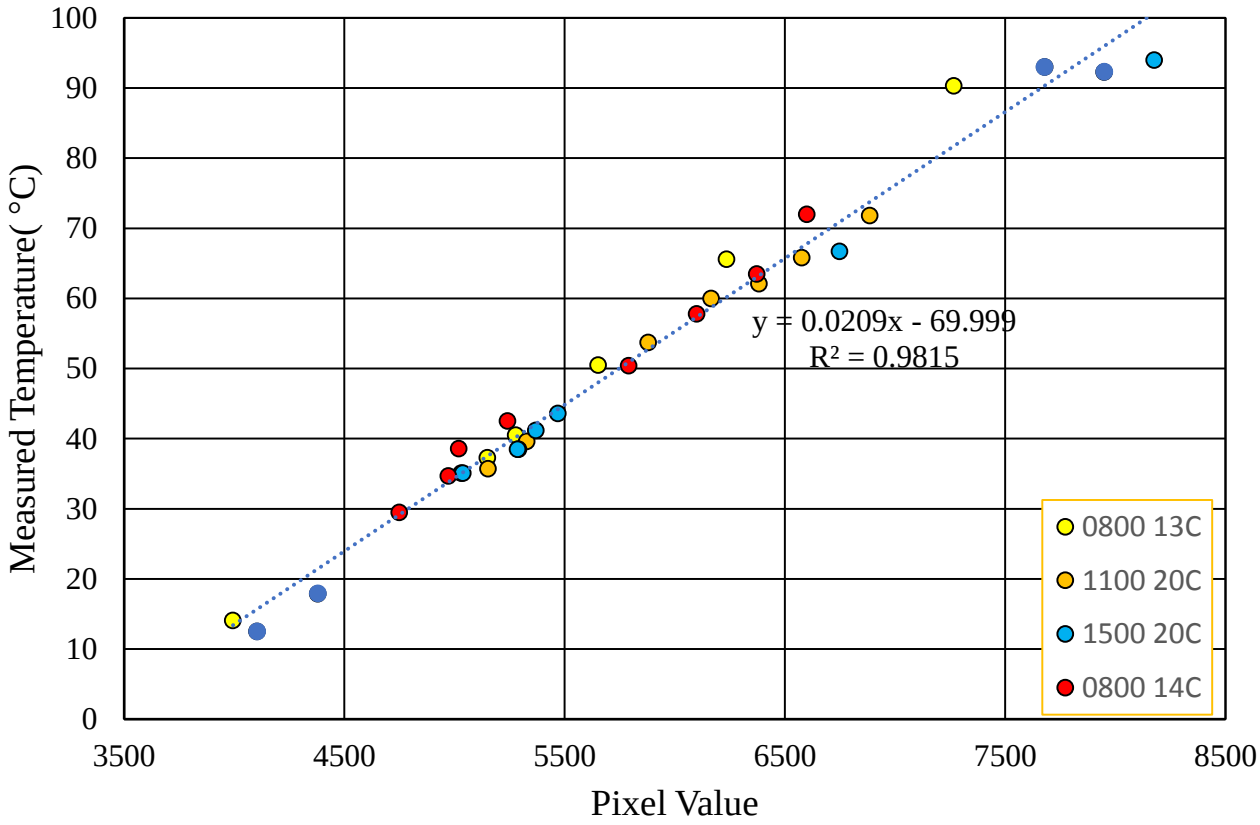


Figure 7: Thermal camera calibration. Points are colour coded according to the time of day and ambient temperature during calibration flight. Line of best fit and equation are for all points. Standard error = 2.3 °C (for measurements <80°C).

## 3 DISCUSSION AND CONCLUSIONS

Recent advances in drone technology, combined with light weight thermal sensors provide a new method for mapping volcanic and geothermal areas at high resolution. However, studies to date have reported only single thermal images (Amici et al., 2013), or very small mosaics without temperature calibration. Our results greatly expand upon previous reports in terms of area (2.2 $km^2$), and by providing temperature calibration, which has allowed an estimate of heat flow.

Our results are important because they show this approach provides a viable alternative to crewed aircraft, at least at the scale of this survey. Depending on survey size and drone type, drones may offer a more economic survey platform than crewed aircraft. They can also fly slower, at much lower altitudes, safely allowing higher resolution imagery (for a given sensor).

The temperature calibrated imagery presented here represents a mosaic of nearly 6000 thermal images captured by drone over a period of 2 weeks. To our knowledge, this is the first square-km-scale, temperature calibrated and georeferenced image of a geothermal area ever produced by a drone equipped with a thermal camera. Temperature calibration and georeferencing of imagery provides the potential for more accurate and reproducible surface heat flow surveying of volcanic and geothermal areas. This has potential applications in volcanic monitoring (Harris, 2013; Vilardo et al., 2015), geothermal exploration (Muffler and Cataldi, 1978), hydrothermal reservoir modelling (O'Sullivan et al., 2001; O'Sullivan et al., 2009) and environmental monitoring (Allis, 1981; Bromley and Hochstein, 2000; Óladóttir and Fridriksson, 2015). Our study demonstrates there are no technical barriers preventing the use of drones to produce accurate thermal and visible maps of large, inaccessible geothermal areas

For non-thermal imagery, the ground resolution (4cm) and horizontal position error (~10cm) are comparable to commercially produced LiDAR and aerial imagery obtained from crewed aircraft.

Calibrated thermal imagery and Monte Carlo analysis provided a mean total surface heat loss of 43 ± 12 MW for thermal lakes and streams in the survey area, for the survey time period. The standard deviation (12 MW) results from meteorological variations expected during the survey period (ambient air temperature, wind speed, humidity, barometric pressure).

The mean surface heat loss 43 ± 12 MW is a probably a minimum, as a small proportion of thermal water is not visible from above (e.g. obscured by vegetation). This value is for evaporation, conduction and radiation; it does not consider advective heat loss associated with ebullition, or advective heat loss associated with the Otamakokore stream flow (Bibby et al., 1995), which comprises nearly all surface out-flow from the survey area (43 MW, Glover et al., 1992)(46MW; Healy, 1952). Assuming a similar heat flow today, the total heat loss for the Waikite survey area averaged ~86MW during the survey period.

**ACKNOWLEDGMENTS**

We would like to acknowledge the New Zealand Department of Conservation, Penoak Farm, Ngati Tahu-Ngati Whaoa Runanga, Ngati Raukawa, Waikite Valley Thermal Pools, GNS Science, Waikite Landcorp Farm, ICI Cameras and The University of Auckland.

**REFERENCES**

Allis, R. G. (1981). Changes in heat flow associated with exploitation of Wairakei geothermal field, New Zealand. *New Zealand Journal of Geology and Geophysics*, *24*(1), 1-19.

Amici, S., Turci, M., Giulietti, F., Giammanco, S., Buongiorno, M. F., La Spina, A., & Spampinato, L. (2013). Volcanic environments monitoring by drones mud volcano case study. International Archives of the Photo-grammetry, Remote Sensing and Spatial Information Sciences, *UAV*, *1*, W2.

Berryman, K., Villamor, P., Nairn, I., Van Dissen, R., Begg, J., & Lee, J. (2008). Late Pleistocene surface rupture history of the Paeroa fault, Taupo rift, New Zealand. New Zealand Journal of Geology and Geophysics, *51*(2), 135-158.

Bibby, H. M., Glover, R. B., & Whiteford, P. C. (1995). The Heat Output of the Waimangu, Waiotapu-Waikite and Reporoa Geothermal Systems (NZ): Do Chloride Fluxes Provide an Accurate Measure? (No. GEO-PROC-95-02). Kelburn Research Centre, IGNS, Wellington, NZ; Wairakei Research Centre, IGNS, Taupo, NZ.

Bromley, C. J., & Hochstein, M. P. (2000). Heat transfer of the Karapiti fumarole field (1946-2000). In *Proceedings of the New Zealand Geothermal Workshop* (pp. 87-92).

Dawson, G.B. (1964). The nature and assessment of heat flow from hydrothermal areas. NZ Journal of Geology and Geophysics, Volume 7, pages 155-171.

Dawson, G. B., & Dickinson, D. J. (1970). Heat flow studies in thermal areas of the North Island of New Zealand. *Geothermics*, *2*, 466-473.

Fonstad, M. A., Dietrich, J. T., Courville, B. C., Jensen, J. L. and Carbonneau, P. E. (2013). Topographic structure from motion: a new development in photogrammetric measurement. Earth Surf. Proc. Land, 38: 421–430. doi: 10.1002/esp.3366.

Fridriksson, T., B. R. Kristjánsson, H. Ármannsson, E. Margrétardóttir, S. Ólafsdóttir, and G. Chiodini (2006). $CO_2$ emissions and heat flow through soil, fumaroles, and steam heated mud pools at the Reykjanes geothermal area, SW Iceland, Appl. Geochem., 21, 1551-1569.

Glover, R. B., Klyen, L. E., & Crump, M. E. (1992). Spring chemistry of the Waikite-Puakohurea thermal area. New Zealand Geothermal Workshop 1992 Proceedings.

Harris, A. (2013). Thermal Remote Sensing of Active Volcanoes: A User's Manual. Cambridge University Press.

Harvey, M.C., Pearson, S., Alexander, K.B., Rowland, J. & White, P. (2014). Unmanned aerial vehicles (UAV) for cost effective aerial orthophotos and digital surface models (DSMs). New Zealand Geothermal Workshop 2014 Proceedings.

Harvey, M. C., Rowland, J. V., & Luketina, K. M. (2016). Drone with thermal infrared camera provides high resolution georeferenced imagery of the Waikite geothermal area, New Zealand. *Journal of Volcanology and Geothermal Research*, *325*, 61-69.

Harwin S, Lucieer A. (2012). Assessing the Accuracy of Georeferenced Point Clouds Produced via Multi-View Stereopsis from Unmanned Aerial Vehicle (UAV) Imagery. Remote Sensing; 4(6):1573-1599.

Healy, J. (1952). Waikite Hot Springs - to inspect the Waikite thermal area and assess its geothermal resources. *DSIR Report*, November 1952. Rotorua.

NIWA (2015) NIWA National Climate Database. http://cliflo.niwa.co.nz/

McGonigle, A. J. S., Aiuppa, A., Giudice, G., Tamburello, G., Hodson, A. J., & Gurrieri, S. (2008). Unmanned aerial vehicle measurements of volcanic carbon dioxide fluxes. Geophysical research letters, *35*(6).

Muffler, P., & Cataldi, R. (1978). Methods for regional assessment of geothermal resources. *Geothermics*, *7*(2), 53-89.

Óladóttir, A. A., & Friðriksson, Þ. (2015). The Evolution of CO2 Emissions and Heat Flow through Soil since 2004 in the Utilized Reykjanes Geothermal Area, SW Iceland: Ten Years of Observations on Changes in Geothermal Surface Activity. Proceedings World Geothermal Congress 2015, Melbourne, Australia.

O'Sullivan, M. J., Pruess, K., & Lippmann, M. J. (2001). State of the art of geothermal reservoir simulation. Geothermics, *30*(4), 395-429.

O'Sullivan, M. J., Yeh, A., & Mannington, W. I. (2009). A history of numerical modelling of the Wairakei geothermal field. Geothermics, *38*(1), 155-168.

Robert, C., & Casella, G. (2013). Monte Carlo statistical methods. Springer Science & Business Media.

Sorey, M. L., & Colvard, E. M. (1994). Measurements of heat and mass flow from thermal areas in Lassen Volcanic National Park, California, 1984-93 (No. 94-4180-A). US Geological Survey; USGS Earth Science Information Center, Open-File Reports Section.

Vilardo, G., Sansivero, F., & Chiodini, G. (2015). Long-term TIR imagery processing for spatiotemporal monitoring of surface thermal features in volcanic environment: A case

study in the Campi Flegrei (Southern Italy). Journal of Geophysical Research: Solid Earth, 120(2), 812-826.

Westoby, M. J., Brasington, J., Glasser, N. F., Hambrey, M. J., & Reynolds, J. M. (2012). 'Structure-from-Motion' photogrammetry: A low-cost, effective tool for geoscience applications. Geomorphology, 179, 300-314.